Applied Catalysis B: Environment and Energy 345 (2024) 123692

Contents lists available at ScienceDirect

Applied Catalysis B: Environment and Energy

journal homepage: www.elsevier.com/locate/apcatb

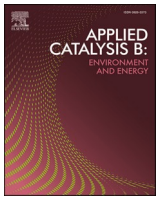

Elucidating charge-transfer mechanisms and their effect on the light-induced reactivity of metastable MIL-125(Ti)

Rassu Pietro [a], Cappai Luca [c], Stagi Luigi [b], Liu Ruirui [a], Enzo Stefano [c], Mulas Gabriele [c], Garroni Sebastiano [c], Malfatti Luca [b], Innocenzi Plinio [b], Ma Xiaojie [a,*], Wang Bo [a,*]

[a] School of Chemistry and Chemical Engineering, Beijing Institute of Technology, 5 South Zhongguancun Street, Beijing 100081, China
[b] Dipartimento di Scienze Biomediche, Università degli Studi di Sassari, Viale S. Pietro 43C, Sassari 07100, Italy
[c] Dipartimento di Scienze Chimiche, Fisiche, Matematiche e Naturali, Università degli Studi di Sassari, Via Vienna 2, Sassari 07100, Italy

ARTICLE INFO

Keywords:
Metal-organic frameworks
Charge-transfer mechanisms
Photocatalysis
Hydroxylation

ABSTRACT

Alcohol and water photooxidation reactions are employed in concert with optical spectroscopy analyses to demonstrate the occurrence of multiple and distinctive charge-transfer (CT) mechanisms in the environmental photocatalyst MIL-125(Ti). The contribution of ligand-to-metal CT (LMCT) mechanisms increases at wavelengths lower than 320 nm while that of node oxygen-to-metal CT (OMCT) mechanisms increases at longer wavelengths. The localization of photogenerated holes on different atoms leads to a selective reactivity of the framework depending on the mechanism and, during hydroxylation processes, to its spontaneous transition to the isostructural MIL-125-OH(Ti) and the development of an additional LMCT mechanism with a long-lived emission. Furthermore, a previously unidentified and extrinsic CT mechanism is spectroscopically related to the formation of terephthalate-based oligomers. The coexistence of distinctive CT mechanisms in MIL-125(Ti) implies their critical role in catalyst efficiency, and mastering them proves to be a powerful and simple strategy to produce the valuable MIL-125-OH(Ti).

1. Introduction

Metal-organic frameworks (MOFs) [1] are an emerging class of porous hybrid inorganic-organic materials based on transition metal oxides with promising prospects both in the environmental, industrial and energy fields [2–9]. Indeed, their long-range ordered structures, high surface area, density of catalytic sites, and structural flexibility make them valid and potentially superior alternatives to other classic homogeneous and heterogeneous compounds for the development of efficient and stable photocatalytic systems. However, the extensive connectivity of their distinctive structural elements can complicate the evaluation of whether the electronic structure and physical properties of these compounds are amenable to those of a molecular array or solid-state material [10–16]. Contributions made by the respective components to the electronic properties of the MOF can vary significantly depending on their interactions (especially under light irradiation), preventing the development of rationally designed materials and leading to potential misunderstanding about their reaction mechanisms [17]. Furthermore, processes of charge transfer (CT), fundamental during photocatalytic reactions [18,19], often differ in coordination polymers from those developed in their simple molecular components. Firstly, coordination bonding can alter the electronic density of the building units relative to their simple molecular form; secondly, the localization of building units at periodic distances prevents interactions comparable to those of free species in solution or in the solid state. It follows that the analysis of CT in MOF photocatalysts (through advanced characterizations or density functional theory calculations) is fundamental to foster a deep understanding of the correlation between CT mechanisms and catalytic unit activity, leading to a rational and exhaustive reactivity of their components, to the development of novel photocatalytic systems and a large-scale industrialization of the photocatalytic processes [17].

Among environmental and industrial photocatalytic MOFs, MIL-125 (Ti) ($Ti_8O_8(OH)_4(BDC)_6$) (BDC: terephthalate) is of great interest as the first carboxylate-based Ti-MOF and progenitor of a family of high-impact isostructural and photocatalytic MOFs [20–30]. Most of the literature suggests that the photoreactivity of this MOF depends on a single ligand-to-metal CT (LMCT) mechanism describable through

* Corresponding authors.
E-mail addresses: xiaojiema@bit.edu.cn (M. Xiaojie), bowang@bit.edu.cn (W. Bo).

https://doi.org/10.1016/j.apcatb.2024.123692
Received 19 September 2023; Received in revised form 5 December 2023; Accepted 1 January 2024
Available online 4 January 2024

comparison of models to known and reproducible experiments, or a higher level of theory [10,12,31–35]. Given the notable contribution of Ti-based nodes to its photoexcitation mechanisms, we instead think of MIL-125 as a crystalline "MOF-analogue" of both bulk and molecular Ti-based systems, with similar photoreactivity. In these Ti-based systems the absorption of light leads to the migration of excited electrons to Ti 3*d* orbitals while photo-generated electron holes remain in the O 2*p* orbitals (bulk TiO_2) or in a combination of O and C 2*p* orbitals (molecular Ti-oxo clusters) [36–38]. In the first case the donor/acceptor (D/A) species are entirely localized in the inorganic cluster and the delocalization of charge carriers proceeds via oxygen-to-metal charge transfer (OMCT) mechanisms; in the second case the D/A species involve the interaction between both inorganic and organic building units, and the delocalization proceeds via LMCT mechanisms. However, up to now, an experimental demonstration of the OMCT mechanisms in the case of MIL-125 has not yet been proposed while the LMCT mechanisms have been widely discussed [10,12,13,31,32,34,39]. In addition, we did not find detailed experimental studies correlating the generation of charges with the unfolding of multiple photo-induced CT mechanisms in a single MIL-125 MOF. Theoretically, multiple CT mechanisms can develop in a MOF with distinctive D atoms and sufficient energy for their respective exciton generation. The generation of charges and their reactivity is expected to depend both on the properties of the individual D/A species and on those of the whole framework. After all, the properties of MOFs are not simply amenable to those of their single components.

Herein, we combine spectroscopic analyses and redox experiments to determine how multiple CT mechanisms influence the photogeneration and reactivity of charge carriers in MIL-125. Each CT mechanism involves a specific localization of charges at the molecular level which can be correlated experimentally with the redox activity of the building units. Firstly, we analyze the effective photoexcitation of MIL-125 at wavelengths both inside and outside the absorption/excitation range of organic ligands (i.e. via LMCT and OMCT) during experiments of deaerated alcohol photooxidation. Similar experiments (essential for a sustainable/green transportation economy and for the production of higher-value commodity chemicals [40–42]) are commonly used in Ti-based coordination polymers to determine the catalytic nature of their Ti-oxo clusters, their efficient acquisition of charged electrons e^-, and the formation of distinctive Ti^{3+} species [17,20,43–45]. However, to date we have not found any studies relating the formation of these Ti^{3+} states to the selective photoexcitation of distinctive molecular components in MIL-125. Secondly, we investigate the reactivity of MIL-125 once photogenerated holes h^+ are localized in node O atoms (OMCT) or in a combination of ligand O and C atoms (LMCT) during experiments of water photooxidation (essential for multiple environmental applications, the production of solar hydrogen and valuable organic compounds [46–51]) and hydroxylation of BDC ligands to 2-hydroxyterephthalate (BDC-OH) via electrophilic aromatic substitution (EAS). Until now it had not been considered that photogenerated holes could be isolated on multiple building units and that this entailed different reactivity in MIL-125 as a function of the CT mechanism; in fact, most of the reported studies are mainly focused on the simple reactivity of electron holes and their lifetimes [26,31,32,35,52,53]. This is the first time that such a theory has been proposed and verified both spectroscopically and experimentally. Moreover, its investigation by luminescence spectroscopy reveals additional and unprecedented CT mechanisms in MIL-125, attributable to its spontaneous phase transition to MIL-125-OH and to the formation of BDC-based oligomers. It follows that at least three significant CT mechanisms are identified in the building units of metastable MIL-125 (OMCT in the Ti-oxo clusters, LMCT between the Ti-oxo clusters and BDC or BDC-OH ligands), and a fourth extrinsic appearing during the hydrolysis of the framework and the formation of BDC-based oligomers (Fig. 1).

This study further progresses the body of work reported to date by using in concert spectroscopic analysis with photoredox experiments to investigate the coexistence of multiple, distinctive, and light-regulated

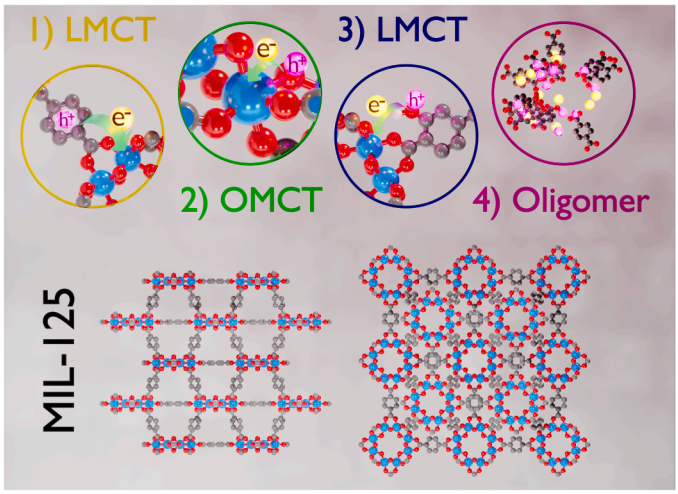

Fig. 1. The four CT mechanisms identified in the molecular components of MIL-125(Ti) under light irradiation (color code: Ti, blue; C, dark grey; O, red; H, white). (1) LMCT from BDC to Ti-oxo cluster; (2) OMCT from oxygen to titanium atoms; (3) LMCT from BDC-OH to Ti-oxo cluster; (4) CT between BDC-based oligomers. Photoexcited electrons are represented as luminous spheres and their movement with green arrows. Bulk crystal structure of the terephthalate-based MIL-125(Ti) (below) is shown in orientation along the A- and C-crystal axes.

CT mechanisms in the molecular components of the environmental photocatalyst MIL-125(Ti). These results confirm that the properties of MOFs are not simply amenable to those of a simple molecular array or a solid-state material as the localization of building units at periodic distances and the coordination bonds significantly alter their molecular photoreactivity. The integration of BDC ligands in ideally pure MIL-125 completely quenches their oligomer interactions, confining much of their photoreactivity and LMCT mechanisms at shorter wavelengths while increasing contributions of inorganic nodes and OMCT mechanisms at longer wavelengths. In addition, unprecedented CT mechanisms are spectroscopically identified during the spontaneous phase transition of metastable MIL-125 to isostructural MIL-125-OH or during the formation of BDC-based oligomers. These results entail a potential change in reactivity (both efficiency and selectivity) of the photocatalyst depending on the wavelength employed and the activated CT mechanism, thus suggesting the need for further investigations in this regard. In addition, controlling photoinduced CT mechanisms turned out to be a simple approach for fine-tuning both structural and optical properties of MIL-125 MOF in a controlled and rational way.

In conclusion, experimentally understanding the correlation between CT mechanisms and catalytic unit activity (e.g. via charge/radical scavenging and luminescence lifetime decay experiments) was paramount to delineate for the first time both the metastable nature of the MOF and the presence of extrinsic CT mechanisms, and to define new potential study objectives for the application of photocatalytic MOFs in research fields such as the environmental and industrial ones.

2. Experimental

2.1. Materials and methods

All starting materials and solvents were purchased from commercial suppliers (Sigma-Aldrich, Alfa Aesar, Aladdin Chemical Co. Ltd, Beijing Chemical Reagent Company, etc.) and used without further purification, unless otherwise specified. All reactions were performed at laboratory ambient conditions, without taking any specific precautions unless otherwise specified (e.g. oxygen and atmospheric humidity were not excluded from the reaction systems).

2.2. Synthesis of MIL-125(Ti)

The procedure is an adaptation of the one originally developed by Dan-Hardi and colleagues [20]. Initially, 250 mg of terephthalic acid (H_2BDC) (Sigma-Aldrich) were dissolved in 4.5 mL of dimethylformamide (DMF)(Sigma-Aldrich); then 0.5 mL of methanol (Sigma-Aldrich) and 0.35 mL of titanium(IV) butoxide (Sigma-Aldrich) were added to the solution in succession and under stirring. The mixture was then subjected to sonication for 15 min before being transferred to a Teflon liner autoclave and put in a digestion bomb at 150 °C for 16 h. After cooling, the white crystalline powders were recovered via centrifugation, washed three times with DMF, and solvent exchanged three times with methanol. Finally, the recovered powders were dried in the oven at 60 °C for one night.

2.3. Characterizations

PXRD. Powder X-ray diffraction (PXRD) analyses were performed on a Rigaku SmartLab X-Ray diffractometer with Cu-Kα radiation 1.54178 Å and a graphite monochromator in the diffracted beam. PXRD patterns were recorded from 5° to 30° (2θ) with a step size of 0.02°, scan rate of 10 deg/min. and a scan resolution of 0.0002. Semiquantitative evaluation of phase abundance and structural features were obtained for the PXRD patterns by nonlinear least-square refinement procedure, according to Rietveld method, and using the MAUD (Materials Analysis Using Diffraction) software.

ATR FTIR. Attenuated total reflectance (ATR) mode was used in the infrared spectral range with an interferometer Bruker infrared Vertex 70 v to record the spectra of the powders between 4000 and 400 cm^{-1} by averaging 128 scans with 4 cm^{-1} resolution. The background was measured using the clean ATR crystal.

Porosimetry. Adsorption and desorption isotherms were recorded at 77 K by using Quantachrome Instrument ASiQMVH002–5 and N_2 as probe gas. The measurements were conducted after pretreating samples by heating them under vacuum at 150 °C for 12 h. All samples were tested with nitrogen (99.9995 %).

UV-Vis. UV–Vis absorption spectra of H_2BDC and sample powders well-dispersed in EtOH or H_2O were collected from 220 to 800 nm using a Nicolet Evolution 300 spectrophotometer.

Photoluminescence. The three-dimensional fluorescence mapping (excitation–intensity emission) of the powders dispersed in ethanol or in solid state was performed using a Horiba Jobin Yvon FluoroMax-3 spectrofluorometer and a 450 W xenon lamp as the excitation source. Maps of the powders dispersed in solution and under continuous stirring were collected with an excitation range of 280 – 400 nm and an emission range of 295 – 440 nm, with a 2 nm slit for excitation and emission, and an integration time of 0.7 s; maps of the powders packed in the sample holder were collected with an excitation range of 270 – 440 nm and an emission range of 286 – 500 nm, with a 2 nm slit for excitation and emission, and an integration time of 0.7 s.

Emission spectra at fixed excitation wavelengths of the powders dispersed in solution and under continuous stirring were collected in a range of 320 to 550 nm, with a 2 nm slit for both excitation and emission, and an integration time of 0.7 s.

Luminescence decay lifetime of the different samples was recorded using an HORIBA NanoLED pulsed diode light source with peak wavelength at 266 nm and a pulse duration < 1.2 ns. BDC-saturated solutions were prepared by dissolving H_2BDC in milli-Q water (pH 7). Meanwhile MIL-125 and MIL-125-OH dispersions were prepared by dilution in ethanol and not in water to avoid further reaction during measurement.

Electron Paramagnetic Resonance. EPR spectra of the powder dispersions were performed with a Bruker EMXplus spectrometer.

2.4. Photoredox experiments

2.4.1. Photooxidation of alcohols

In a conventional experiment, MIL-125(Ti) powders of known mass (1.6–1.8 mg) were transferred to a quartz UV-Vis cuvette together with a magnetic stir bar. The cuvette thus prepared was loaded in the glovebox in an argon atmosphere and 2 mL of deaerated EtOH were poured into it. At this point the cuvette was closed with a Teflon cap, sealed with multiple layers of parafilm tape, removed from the glovebox and parafilmed again. The sealed cuvette was sonicated for 5 min and kept under magnetic stirring for one hour, so as to ensure the homogenous dispersion of the MOF in solution and the adsorption of the alcohol. Meanwhile, a light source (Solar Simulator or LED light) was turned one and allowed to equilibrate for at least 30 min. Thus, the cuvette with the MOF dispersion was set in front of the light source on a stirring plate, under constant agitation and cooling ventilation. The sample was irradiated for a set amount of time, and subjected to UV-Vis spectroscopic analysis to evaluate the rate of photoreduction.

2.4.2. Photooxidation of water

In a conventional experiment, MIL-125(Ti) powders of known mass were transferred to a quartz UV-Vis cuvette together with a magnetic stir bar and a fixed volume of water solution at the desired pH value. The cuvette thus prepared was closed with a Teflon cap and sealed with multiple layers of parafilm tape; thus, it was sonicated for 5 min and kept under magnetic stirring for one hour, so as to ensure the homogenous dispersion of the MOF in solution and the adsorption of the solution. Afterwards, the cuvette with the MOF dispersion was set in front of the light source on a stirring plate, under constant agitation and cooling ventilation. The sample was irradiated for a set amount of time, and subjected to PL spectroscopic analysis to evaluate the rate of hydroxylation in the hybrid polymer dispersion.supporting information

Scavenger quenching experiments. The scavengers used were EtOH for photogenerated electron holes h^+, $AgNO_3$ (Sigma, >=99 %) for photoexcited electrons e^-, benzene and 5,5-dimethyl-pyrroline-*N*-oxide (DMPO) for hydroxyl radicals. The species were added into the water suspension before illumination. Samples were irradiated for a set amount of time, and subjected to PL analysis to evaluate the rate of water photooxidation and the generation of hydroxyl radicals •OH.

2.4.3. Light sources

Experiments for the photoexcitation of both the inorganic and organic building units of the sample were carried out using an Abet Technologies Sun 2000 Solar Simulator equipped with a 150 Watt Xenon short arc lamp and an irradiating power of 1 sun (AM 1.5). Experiments for the selective light-induced excitation of the sample components were carried out using a Zolix LED power supply for industrial and biological research applications, equipped with a light source model M310L (>100 mW), in a range of 295–335 nm and with a maximum at 310 nm, or a light source model M365L (>420 mW), in a range of 350–400 nm and with a maximum at 365 nm (emission spectra reported in Fig. S7). The irradiance of the LED lights was measured with an ILT550 spectroradiometer from International Light Technologies.

3. Results and discussion

3.1. Optical characterizations

To gain an initial perspective on the photo-induced CT mechanisms in MIL-125, the optical properties are investigated by comparing UV-Vis absorption spectra of the sample and organic ligands as dispersions in ethanol (EtOH) (Fig. 2a, S4). MIL-125 dispersion has a high absorbance entirely localized in the UV part of the spectrum, with two maxima (λ_{max}) at 238 and 318 nm, and a band edge around 375 nm. H_2BDC dispersion is similarly characterized by two distinctive absorption bands in the UV part of the spectrum; however, its λ_{max} are located at 238 and

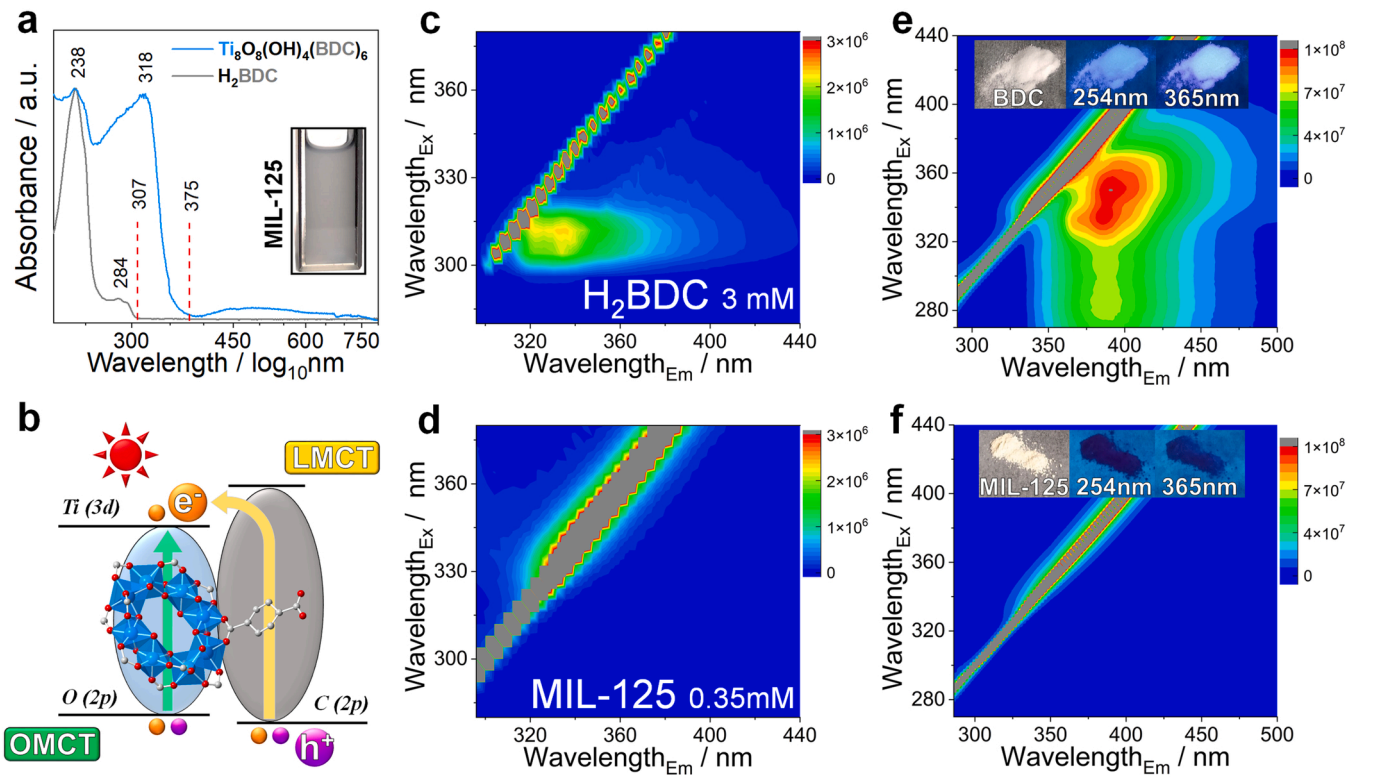

Fig. 2. (a) UV-Visible absorption spectra of the MIL-125(Ti) powder sample (blue line-top) (≈0.5 mg mL^{-1}; 0.35 mM) and organic ligand H_2BDC (black line-bottom) dispersed in EtOH. Inset: picture of MIL-125(Ti) powders dispersed in EtOH. (b) Schematic illustration of the CT processes between the molecular orbitals that make up the electronic structure of MIL-125(Ti). 2D (excitation (y)–emission (x)-intensity (false color scale)) of (c) H_2BDC (≈0.5 mg mL^{-1}; 3.0 mM) and (d) MIL-125(Ti) (≈0.5 mg mL^{-1}; 0.35 mM) dispersions in EtOH. 2D (excitation (y)–emission (x)-intensity (false color scale)) of (e) H_2BDC and (f) MIL-125(Ti) dried powders, and (inset) related photographs under irradiation with sunlight or fixed wavelength lamps (λ_{max} set at 254 and 365 nm).

284 nm, and the band edge is around 307 nm. Accordingly, the photoexcitation of BDC ligands comes into play to a greater extent at wavelengths lower than 307 nm and gradually becomes smaller as wavelengths grow beyond 310 nm. Thus, the light absorption of the polymer in the 310–375 nm range could mostly result from an alternative contribution of D species mainly localized in the octameric nodes rather than in the ligands (Fig. 2b). This, however, seems to deviate from previously conducted calculations [12,34,39,54]; according to their results, the photoexcitation of MIL-125 is expected to proceed mainly through LMCT processes and without any involvement from OMCT mechanisms.

Photoluminescence (PL) spectroscopy measurements further ascertain the effective excitation and recombination behavior of photogenerated charges. As reported in both the 2D dispersion and solid-state PL maps (Fig. 2c,e), H_2BDC is highly fluorescent under these experimental conditions, and has a highly asymmetrical emission mark (indicative of multiple emissive species rather than single ones). However, the excitation range of BDC species gradually decreases with increasing spacing of the molecules and decreasing their potential interactions (e.g. via aromatic ring stacking or formation of oligomers). The excitation/absorption edges of H_2BDC molecules shifts at wavelengths below 320 nm when the BDC-based species do not have intense electronic interactions with each other (Fig. 2e, S4).

Meanwhile, the BDC species integrated within the crystalline framework of MIL-125(Ti) are coordinated with inorganic Ti_8-oxo clusters that may behave as quenchers, effectively delocalizing the photogenerated polarons and decreasing their luminescent emission. In addition, their localization at precise and repetitive distances in the framework prevents their interaction and favors their non-fluorescent state [55–58]. In accordance with these premises, the 2D fluorescence map of our MIL-125(Ti) sample (0.35 mM) does not show any radiant emission comparably attributable to organic ligands (Fig. 2d,f). This is clearly emphasized in the PL emission spectra and in the photographs (Figs. 2e,2f,S5), where BDC-based powders show dissimilar behavior. This outcome is in good agreement with the assembly of an ideal coordination polymer with a high degree of purity; furthermore, it suggests that photoexcitation of BDC species coordinated to Ti-oxo clusters becomes increasingly unfavorable as the excitation wavelength increases beyond 310 nm. As the band edge at 375 nm is approached, exciton generation in MIL-125 would be primarily attributable to alternative D atoms located at the octameric nodes. Consequently, the coordination polymer is expected to gradually behave more like a molecular array of bulk TiO_2 or Ti-oxo clusters at higher excitation wavelengths.

3.2. Photoredox experiments

3.2.1. Photooxidation of alcohols

Firstly, we use the photooxidation of alcohol molecules to experimentally determine the potential CT mechanisms in MIL-125 and the electron migration to node A atoms. Just like in other Ti-based nanomaterials (both bulk and molecular), oxidation of deaerated alcohols with photo-generated holes induces the formation of stable Ti^{3+} excited states in Ti-MOFs [20,59–65]. These Ti^{3+} states are characterized by specific absorptions in the visible part of the spectrum. Consequently, irradiation of the sample at wavelengths within or outside the absorption/excitation range of the organic building units (Fig. 2a) indicates whether the photo-oxidation of alcohols by MIL-125 depends solely on LMCT mechanisms.

Exposure of MIL-125(Ti) in a deaerated EtOH solution to the radiation of a solar simulator ($\lambda > 300$ nm) is followed by an increasing color change of the crystalline powder from white to deep blue-black (Fig. S6), in line with the reduction of ground state Ti^{4+} species to excited Ti^{3+}

species. Apart from the overall increase in absorption related to light scattering and reflection phenomena, absorption spectra display new intense and broad bands in the visible and near-infrared (Vis-NIR) (Fig. 3a), associated with *d-d* transition states (508 nm) and intervalence transition states (612 nm) [20,60–63]. Absorption in the Vis-NIR range increases rapidly during the first hours of irradiation but seems to slow down over time, achieving an almost stable threshold value after more than 19 h of continuous irradiation (Fig. S6) [66].

Photoreduction of the coordination polymer with a light source emitting in the absorption/excitation range of the ligand demonstrates effective transfer of charged polarons to Ti-based nodes via LMCT. Meanwhile, repeating the same experiment with an LED light source emitting well beyond this absorption/excitation range ($\lambda = 365$ nm) similarly induces the oxidation of alcohols and the reduction of Ti-nodes (Fig. 2b,S6). Absorption lineshapes and long-term stability are analogous to those observed when using the solar simulator and, thus, are associated with the optically induced hopping of charged polarons from the Ti^{3+} to Ti^{4+} species. These experimental data imply the efficient redox reaction between MOF and alcohols at wavelengths both inside and outside the absorption/excitation range of organic ligands (i.e. via LMCT or OMCT) (Fig. 3c).

3.2.2. *Photooxidation of water*

Secondly, we use the heterogeneous water oxidation to experimentally demonstrate the coexistence of multiple CT mechanisms in MIL-125 and the different reactivity of electron holes generated at wavelengths inside and outside the absorption/excitation range of organic ligands (Fig. S7). Whereas both of the previously described mechanisms

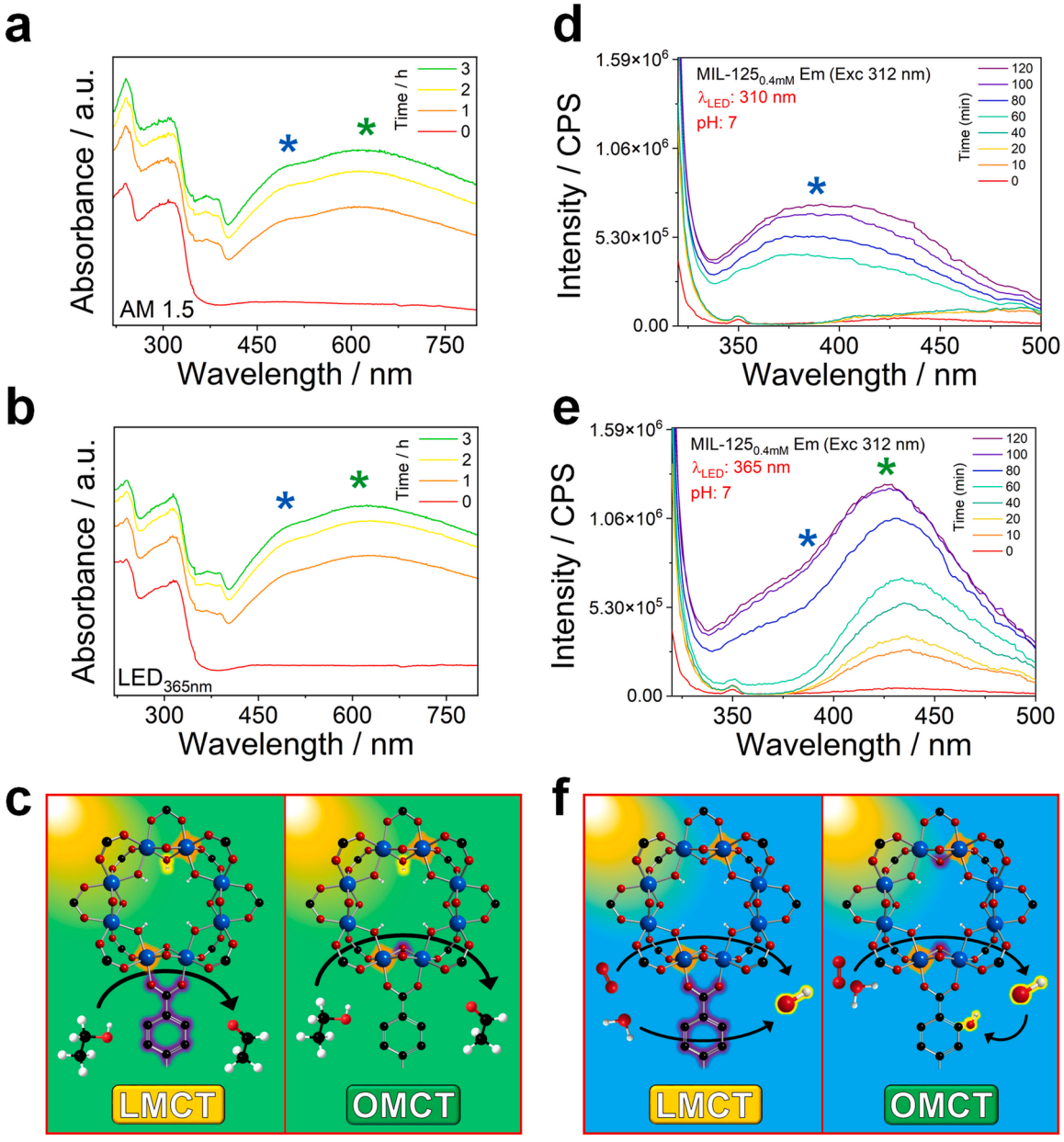

Fig. 3. UV-Vis absorption spectra of MIL-125(Ti) dispersions irradiated with (a) a solar simulator and (b) an LED light source; the new bands with at 508 (blue star) and 612 nm (green star) are respectively related to d-d and intervalence transition states of Ti^{3+} species. (b) Photoluminescence emission spectra of 0.4 mM aqueous MIL-125(Ti) dispersions during a 120-minute long irradiation using LED light sources with λ_{max} set at (d) 310 nm or (e) at 365 nm. The new bands at 383 (blue star) and 426 nm (green star) are respectively related to luminescent BDC-based oligomers and BDC-OH ligands. Schematic representation of (c) ethanol and (f) water photooxidation via LMCT and OMCT mechanisms in MIL-125 (color code: Ti, blue; O, red; C, grey; H, white; photoexcited e^- location, orange halo; photogenerated h^+ location, violet halo; •OH and -OH, yellow halo).

lead to similar Ti^{3+} species, photogenerated holes are assumed to induce different reactivity in the framework depending on their starting D atoms. Hydroxyl radicals •OH (one of the main water oxidation products) can usually react with aromatic molecules such as benzoates through EAS, producing fluorescent species. In this regard, non-fluorescent terephthalate molecules, as highly symmetric "para-carboxy benzoates", produce only one mono-hydroxylated fluorescent isomer via EAS, with well-reported excitation and emission maxima (located at 312 nm and 426 nm, respectively) [55–58]. However, the fact that terephthalate species are structural elements of our photocatalyst implies that, firstly, their reactivity with hydroxyl radicals is significantly influenced by CT mechanisms and how these alter the aromatic electron density; secondly, that the hydroxylation of terephthalate ligands leads to a progressive transition towards the isostructural MIL-125-OH which can be monitored in real time.

PL spectra of aqueous dispersions of MIL-125 (0.4 mM) irradiated with an LED source fixed at 310 nm do not display any clear emission at 426 nm attributable to the hydroxylation of organic ligands (Fig. 3d). On the other hand, a new band with λ_{max} set around 383 nm rises after one hour of irradiation and continuously grows in intensity over time. We associate this last band with PL processes that are extrinsic to the polymer itself and correlated instead to photosensitive interactions between terephthalate species hydrolyzed from it and oversaturating the aqueous medium. In fact, firstly, their emissions are similar to those observed in H_2BDC dispersions (Fig. S4,S8). Secondly, the emission at 383 nm increases in intensity over time both when the coordination

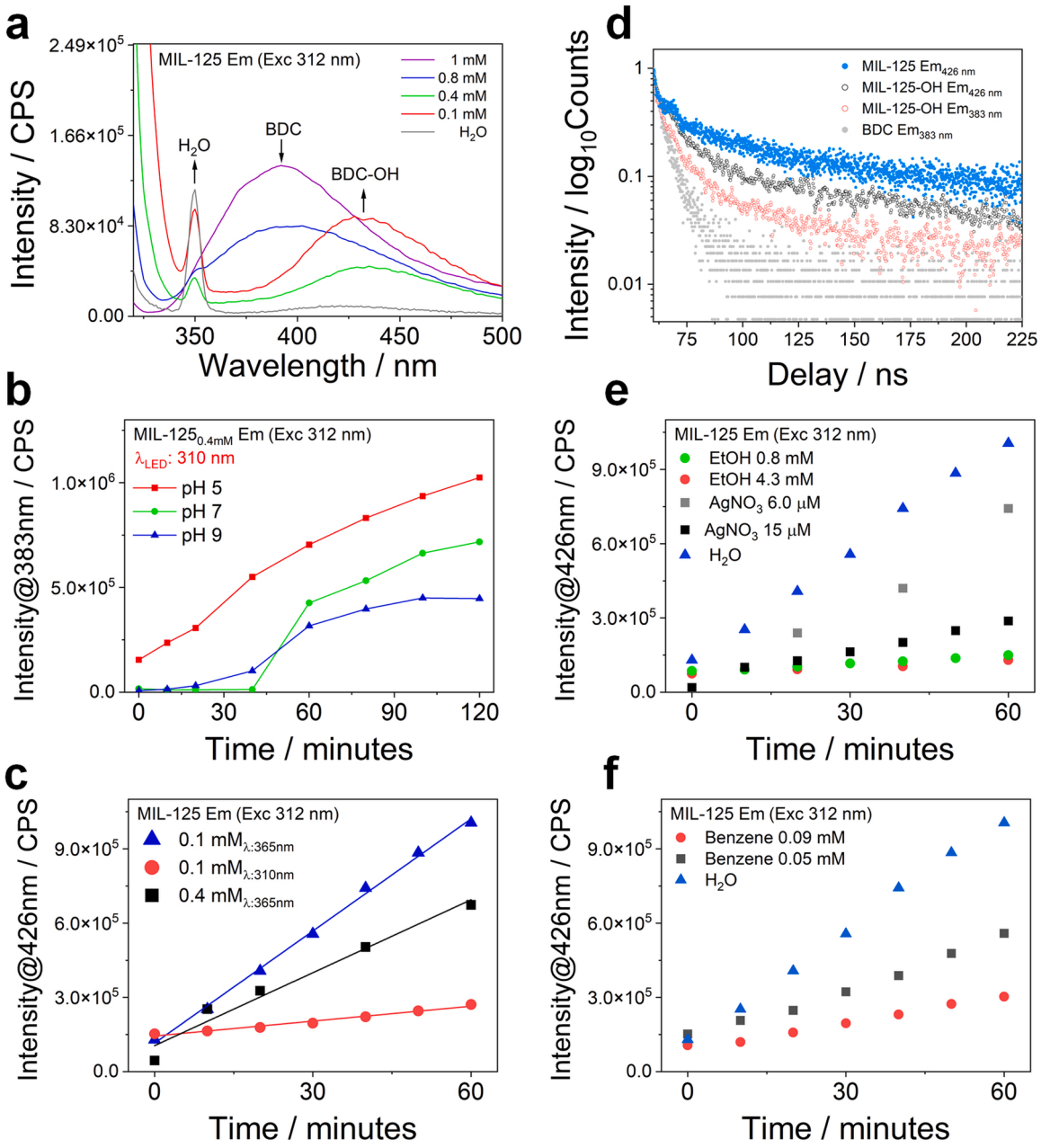

Fig. 4. (a) PL emission spectra of aqueous MIL-125(Ti) dispersions with different molar concentrations and highlighting the emissions of BDC-based oligomers and BDC-OH species in bare MIL-125. (b) Variation of the emission intensity at 383 nm (BDC oligomers) for 0.4 mM MIL-125 dispersions irradiated at 310 nm as a function of the pH value of the solution. (c) Variation of the emission intensity at 426 nm (BDC-OH species) for MIL-125 dispersions irradiated at 310 or 365 nm as a function of molar concentration. (d) Luminescence decay lifetime of post-synthetically hydroxylated MIL-125-OH, pristine MIL-125, and supersaturated BDC aqueous dispersions. PL emission intensity at 426 nm of 0.1 mM MIL-125(Ti) aqueous dispersions, under 365 nm light irradiation and in presence of (e) charge scavengers and (f) hydroxyl radical scavengers.

polymer dispersion is subjected to irradiation and when it is kept in the dark for a long time (Fig. S9). Thirdly, the emission increases with the molar concentration of the polymer dispersed in solution as more terephthalate molecules are hydrolyzed (i.e. faster oversaturation of the solution) (Fig. 4a). Finally, the intensity of the emission varies with the pH of the solution in a similar way to that of BDC molecules as they are poorly soluble in organic solvents and even less in water (Fig. 4b). BDC molecules tend to form luminescent oligomers when partially solubilized (e.g. under acidic conditions) or to remain dispersed as non-luminescent monomers when deprotonated/solubilized (e.g. at neutral or, better yet, basic pH values). Accordingly, the emission at 383 nm grows much more rapidly when MIL-125 dispersions are irradiated under acidic conditions since the coordination polymer is easily hydrolyzed and the organic ligands are weakly soluble (Fig. 4b). On the other hand, a comparable aggregation phenomenon in the polymer dispersion takes much longer when the pH grows to neutral or basic values, as BDC species become increasingly soluble. It therefore follows that, following hydrolysis and independently of light irradiation, any compound based on terephthalate species should form oligomers with CT mechanisms independent from those of the starting compound. What's more, the formation of similar species can be easily detected and investigated via PL spectroscopy, thus ascertaining their mechanisms under different reaction conditions. As far as we know, this is the first time such an extrinsic mechanism is reported and investigated in detail in a coordination polymer and, more specifically, in the case of MIL-125 [26,39,67,68].

Meanwhile, conducting the same experiment with an LED source set at 365 nm provides important evidences on the existence of multiple D species in MIL-125 (Fig. 3e). A band around 383 nm, similar in shape and intensity to that previously observed, appears and grows after one hour of irradiation; this further supports the correlation of the 383 nm emission with mechanisms independent of ligand hydroxylation and radiant light. Per contra, a second band, set at 426 nm and consequently related to the formation of BDC-OH ligands, visibly increases in intensity from the very beginning of the experiment and continues steadily with increasing concentration of hydroxylated species. In addition, the intensity of this band (i.e. the hydroxylation rate) changes over time when the pH of the solution deviates from neutral values (Fig. S10) since the polymer is more stable under neutral pH conditions [69,70]. The various contributions to these luminescent emissions in MIL-125 aqueous dispersions (i.e. the bands at 383 and 426 nm) become clearer to isolate and study by acquiring measurements at different molar concentrations. At concentrations higher than 0.4 mM, the emission bands overlap and the oligomers contribution gets bigger and bigger (Fig. S11c,d); this is due to a faster supersaturation of the aqueous dispersion with hydrolyzed BDC species and possibly interferes with the luminescence itself (Fig. S11d). On the contrary, the emission band at 383 nm completely disappears when the molar concentration drops to around 0.1 mM, leaving only the band at 426 nm clearly visible for spectroscopic determination (Fig. S11a,b) and simplifying detailed analysis of hydroxylation processes. For instance, it is apparently clear that the MOF is already minimally hydroxylated even before irradiation with the light source due to the high reactivity of its inorganic clusters (i.e. there is a natural and slow transition between isostructural MIL-125 and MIL-125-OH even under ambient conditions) (Fig. 4a); the hydroxylation trend of a 0.1 mM dispersion irradiated at 310 and 365 nm becomes more evident and linear compared to a 0.4. mM dispersion (Fig. 4c,S11a); the relevance of aqueous medium saturation with BDC species is also highlighted when performing the hydroxylation at 365 nm with specially saturated solutions (Fig. S12).

The luminescent features of BDC oligomers (383 nm) and MIL-125-OH (426 nm) were further studied spectroscopically via luminescence decay lifetime, using a laser with peak at 266 nm to excite both luminescent species (Fig. 4d). Two different lifetimes τ_1 and τ_2 are extracted by fitting the decay profile of our MIL-125-OH sample. The short-lived τ_1 value (5.4 ns) is related to the BDC-based oligomers since its intensity is greater at 383 nm while the long-lived τ_2 value (31 ns) is instead related to MIL-125-OH since its intensity is greater at 426 nm. The correlations of τ_1 and τ_2 are further confirmed by observing how they match the decay profiles of BDC-supersaturated aqueous solutions and pristine MIL-125 dispersions; in both cases a single τ_n value is found which correctly matches the respective components of the MIL-125-OH dispersion. These results confirm (a) the presence of a BDC oligomer-related component in the emission of MIL-125-OH and (b) the early presence of BDC-OH species in the starting MIL-125 compound (as previously detected in Fig. 4a). In addition, they are reasonably in line with previous theoretical works suggesting slower recombination in isostructural MIL-125-X MOFs (X: OH, NH_2, SH) due to the spatial separation of electrons in Ti(3*d*) orbitals and holes in X orbitals within the organic building units [34,39].

Finally, the addition of scavenging reagents provides important evidences on the reaction mechanisms and potential further applications. The use of charge scavengers supports the involvement of both polarons in the terephthalate hydroxylation as PL intensity clearly decreases with their addition (Fig. 4e,S13). This result confirms the relevance of MIL-125 as a photocatalyst for environmental/industrial application and, in particular, for the effective oxidation of alcohols even in the presence of other adsorbed species. At the same time, the use of hydroxyl scavengers further correlates the emission at 426 nm with the formation of hydroxyl radicals (Fig. 4f,S14). Besides, it reveals how the generation of hydroxyl radicals can potentially be employed to produce valuable organic compounds (e.g. hydroxylation of benzene into phenol). In particular, the addition of 5,5-dimethyl-pyrroline-*N*-oxide (DMPO) as spin trapping agent in a deaerated atmosphere demonstrates the generation of free •OH radicals in solution both via OMCT and LMCT mechanism (Fig. S15). It follows that the generation of hydroxyl radicals with MIL-125 MOF does not depend on the CT mechanisms.

It is therefore evident that there are multiple CT mechanisms intrinsic to the MIL-125 MOF and regulating its reactivity. In our specific case, the hydroxylation of aromatic ligands occurs at wavelengths both inside and outside the excitation range of organic linkers. Thus, this outcome further confirms the redox efficiency of the polymer during the water photooxidation reaction, both via LMCT and OMCT mechanisms (Fig. 3f). Furthermore, it could imply a different reactivity of the polymer depending on the light source modulation (e.g. by controlling the irradiance and excitation interval) and the contribution of its specific CT mechanisms. After all, previous reports thoroughly described how different D species and CT mechanisms in MIL-125 isostructural MOFs can lead to the generation of excited states with distinctive lifetimes, reactivity, and reaction products [26,34,35,39]. In agreement with these premises, we find it reasonable to think that the OMCT mechanism is more advantageous than the LMCT one for specific EAS reactions with hydroxyl radicals and for the photooxidation reactions in general.

On the one hand, the electrophilic attack of the hydroxyl radical on the aromatic ring to form the carbocationic intermediate should be generally more difficult to accomplish in MIL-125, given the electron withdrawing effect (EWE) of both carboxylate substituents and coordinated Ti-oxo clusters (Fig. S16). The transfer of photoexcited electrons to the Ti-based nodes via LMCT would further deplete the π-electron system, increasing the free-energy required to access the intermediate arenium ion state and discouraging oxidation/electrophilic substitutions in the aromatic moiety. Even after the transfer of the photogenerated holes, the electrophilic attack on the aromatic ligands during LMCT could still be disadvantaged since, in addition to being the first and rate-determining step, it is notoriously slow (probably slower than the photoexcitation process) [71]. In addition, increasing the contribution of the LMCT mechanism by decreasing the light source excitation wavelength could in itself prove disadvantageous for the MIL-125 framework and facilitate the overoxidation of its ligands. Despite their well-documented stability, terephthalate species can generally incur photoinduced oxidation processes at increasingly lower excitation wavelengths and in the presence of suitable photocatalysts [72–75];

similar effects have been observed even when the terephthalate species were integrated into multiple hybrid coordination frameworks [76]. It follows that LMCT mechanisms, whose contribution increases at low excitation wavelengths, may be disadvantageous for MIL-125 during reactions of water and alcohol photooxidation.

On the other hand, photoexcitation of inorganic clusters and promotion of OMCT mechanism should increase the electron density in Ti-based nodes while preserving that of the ligands; this could lead to the decrease of nodes EWE and, during the oxidation of water, to favor the hydroxylation of ligands (Fig. S16). It follows that the OMCT mechanism could be considered more advantageous than the LMCT one for the photocatalytic application of MIL-125. Firstly, it is the only one of the two that can be clearly activated without the involvement of the other; secondly, it allows photogeneration of excitons and activation of the redox capacities of the catalyst with lower energy (i.e. at higher excitation wavelengths); thirdly, the oxidative potential of OMCT mechanisms is capable of producing highly reactive and desirable species (e.g. hydroxyl radicals) even at the band edge of the polymer where absorption is minimal; lastly, the conditions for the activation of the OMCT mechanism appear to be less demanding for the structural integrity of the catalyst.

Thus, these results highlight the importance of deepening the understanding of CT mechanisms and of the localization of photogenerated species in MOFs as, just like in biological systems, they may play a critical role in the efficiency of the catalyst to produce reactive species and control selectivity [17,77,78]. In this specific case, the main reaction species (i.e. charged species and oxygen radicals) are considered fundamental for the application of both environmental photocatalysts based on MOFs (isostructural of MIL-125 and otherwise) and of other chemical nature [24,27,28,79–85]; these species are in fact responsible for the mineralization of organic pollutants in water, for the generation of valuable organic compounds used in agrochemical, industrial and pharmaceutical fields, or for the conversion and storage of energy. Hydroxyl radicals, in particular, are regarded as the most active oxygen species for many photocatalytic processes such as the photodegradation of harmful organic pollutants and the photocatalytic oxidation of water to molecular O_2 [86–93]; thus, the detailed elucidation of their generation and reactions (both with the catalyst surface and with other compounds in solution or adsorbed) is fundamental so as to favor a rational and exhaustive modulation of the catalyst, improving its photocatalytic performance (selectivity and efficiency) during environmental, industrial and clean energy applications.

Incidentally, the photocatalytic hydroxylation of MIL-125(Ti) appears to be a natural transition process between two isostructural MOFs which can be easily accelerated by controlling CT mechanisms. In this regard, this method can also be considered a direct, clean and cost-effective procedure to post-synthetically modify the properties of the coordination polymer. In fact, just like for other M^{4+}-BDC MOFs, the preparation of isostructural MIL-125-OH samples is considered challenging to accomplish solvothermally and without using additional reagents, catalysts, or reaction/purification steps [94–96]. The final product is an isostructural framework of the MIL-125 with new uncoordinated hydroxyl groups which functionalize the aromatic ring of the ligands; these functional groups are capable of further reactions, of forming new bonds, they alter both the chemical environment, the electronic structure and optical properties compared to the parental ones [32,34]. Thus, in addition to having been investigated only superficially with respect to other MOFs (isostructural and not), we believe that MIL-125-OH possesses advantageous properties in multiple fields of application, both alone and combined with other materials, similarly and alternatively to well-known MIL-125-NH_2 [25–30]. In this regard, the clarification and control of photoinduced CT mechanisms in the MIL-125 is revealed as a powerful tool for its simple but effective post-synthetic functionalization and the preparation of valuable isostructural materials with a potential yet to be investigated.

4. Conclusions

This study comprehensively breaks down the CT mechanisms induced under light irradiation in the BDC-based MIL-125(Ti), experimentally outlining the presence of multiple D species with distinctive reactivity. These D atoms can be selectively activated by providing regulated amounts of energy through irradiation. Smaller amounts of energy mostly lead to the photoexcitation of node O atoms and to OMCT mechanisms; higher amounts of energy lead to the preferential excitation of aromatic C atoms and to LMCT mechanisms. Regardless of the energy supplied, both mechanisms can efficiently generate excitons and delocalize photoexcited electrons to node Ti atoms. The efficiency of these distinctive CT mechanisms is confirmed by recording the generation of visible-sensitive Ti^{3+} species within MIL-125 during irradiation at wavelengths both inside and outside the absorption/excitation range of organic ligands. Meanwhile, the effective reactivity of electron holes photogenerated in O or C atoms is ascertained by investigating the photo-induced hydroxylation of coordination polymer ligands at specific emission intervals. Under similar reaction conditions, both mechanisms demonstrate to generate electron holes with an oxidative potential capable of producing highly reactive hydroxyl radicals under light irradiation; the luminescence assigned to BDC-OH species dispersed in solution steadily increases over time when the samples are irradiated at wavelengths both inside and outside the excitation range of organic ligands (i.e. via LMCT and OMCT). However, the OMCT mechanism appears to be more advantageous than the LMCT one as it can be selectively photoinduced under more favorable conditions for photooxidation of water and still produce highly reactive redox states. A more in-depth study of the luminescence properties of polymer dispersions also reveals (a) alternative and intrinsic CT processes connected to its “spontaneous”, albeit minimal hydroxylation, even in ambient conditions, and (b) extrinsic CT mechanisms related to the formation of ligand oligomers in supersaturated BDC solutions. In fact, their luminescence decay profiles have specific τ_n values attributable to the respective luminescent species.

In conclusion, the presence of multiple and coexisting CT mechanisms in photoactive MOFs such as MIL-125(Ti) presupposes a potential reaction selectivity as a function of the energy supplied with the irradiation. The recognition of distinctive D/A species in the same material, spectroscopically and experimentally, is paramount to correctly comprehend their effective reactivity and contribution to photoinduced processes. These photoinduced processes, in fact, determine the catalytic effectiveness of the material and can further modulate its own properties during use. We believe that this study may contribute to a better understanding and characterization of CT mechanisms in MOFs, inspiring future investigations into the impact that multiple and coexisting CT mechanisms may have on the reaction selectivity and efficiency of photoactive MOFs such as metastable MIL-125(Ti) during their applications in the environmental, industrial, or energy fields.

Declaration of Competing Interest

The authors declare that they have no known competing financial interests or personal relationships that could have appeared to influence the work reported in this paper.

Data Availability

Data will be made available on request.

Acknowledgements

This work was financially supported by the National Nature Science Foundation of China [Grant Nos. 22076011, 21971017]; National Key Research and Development Program of China [Grant No. 2022YFC2603700], and Beijing Institute of Technology Research Fund

Program. The authors acknowledge the Analysis and Testing Center of BIT for technical supports, and the GAUSS-CeSAR (Centro Servizi d'Ateneo per la Ricerca) of the University of Sassari for XRD measurements.

Appendix A. Supporting information

Supplementary data associated with this article can be found in the online version at doi:10.1016/j.apcatb.2024.123692.

References

[1] O.M. Yaghi, M.J. Kalmutzki, C.S. Diercks. Introduction to Reticular Chemistry: Metal-Organic Frameworks and Covalent Organic Frameworks, Wiley-VCH Verlag GmbH & Co. KGaA, 2019.

[2] F.-L. Li, Q. Shao, X. Huang, J.-P. Lang, Nanoscale trimetallic metal–organic frameworks enable efficient oxygen evolution electrocatalysis, Angew. Chem. Int. Ed. 57 (2018) 1888–1892.

[3] F.-L. Li, P. Wang, X. Huang, D.J. Young, H.-F. Wang, P. Braunstein, J.-P. Lang, Large-scale, bottom-up synthesis of binary metal–organic framework nanosheets for efficient water oxidation, Angew. Chem. Int. Ed. 58 (2019) 7051–7056.

[4] Q. Wang, Q. Gao, A.M. Al-Enizi, A. Nafady, S. Ma, Recent advances in MOF-based photocatalysis: environmental remediation under visible light, Inorg. Chem. Front. 7 (2020) 300–339.

[5] S. Liu, C. Zhang, Y. Sun, Q. Chen, L. He, K. Zhang, J. Zhang, B. Liu, L.-F. Chen, Design of metal-organic framework-based photocatalysts for hydrogen generation, Coord. Chem. Rev. 413 (2020) 213266.

[6] D. Li, M. Kassymova, X. Cai, S.-Q. Zang, H.-L. Jiang, Photocatalytic CO_2 reduction over metal-organic framework-based materials, Coord. Chem. Rev. 412 (2020) 213262.

[7] Q. Qian, P.A. Asinger, M.J. Lee, G. Han, K. Mizrahi Rodriguez, S. Lin, F. M. Benedetti, A.X. Wu, W.S. Chi, Z.P. Smith, MOF-based membranes for gas separations, Chem. Rev. 120 (2020) 8161–8266.

[8] C.-Y. Liu, X.-R. Chen, H.-X. Chen, Z. Niu, H. Hirao, P. Braunstein, J.-P. Lang, Ultrafast luminescent light-up guest detection based on the lock of the host, Mol. Vib. J. Am. Chem. Soc. 142 (2020) 6690–6697.

[9] C. Du, Z. Zhang, G. Yu, H. Wu, H. Chen, L. Zhou, Y. Zhang, Y. Su, S. Tan, L. Yang, J. Song, S. Wang, A review of metal organic framework (MOFs)-based materials for antibiotics removal via adsorption and photocatalysis, Chemosphere 272 (2021) 129501.

[10] K.T. Butler, C.H. Hendon, A. Walsh, Electronic chemical potentials of porous metal–organic frameworks, J. Am. Chem. Soc. 136 (2014) 2703–2706.

[11] X.-Y. Wu, H.-X. Qi, J.-J. Ning, J.-F. Wang, Z.-G. Ren, J.-P. Lang, One silver(I)/tetraphosphine coordination polymer showing good catalytic performance in the photodegradation of nitroaromatics in aqueous solution, Appl. Catal. B 168-169 (2015) 98–104.

[12] A. Walsh, K.T. Butler, C.H. Hendon, Chemical principles for electroactive metal–organic frameworks, MRS Bull. 41 (2016) 870–876.

[13] J.L. Mancuso, A.M. Mroz, K.N. Le, C.H. Hendon, Electronic structure modeling of metal-organic frameworks, Chem. Rev. 120 (2020) 8641–8715.

[14] N. Kolobov, M.G. Goesten, J. Gascon, Metal–organic frameworks: molecules or semiconductors in photocatalysis? Angew. Chem. Int. Ed. 60 (2021) 26038–26052.

[15] M.-F. Wang, Y. Mi, F.-L. Hu, H. Hirao, Z. Niu, P. Braunstein, J.-P. Lang, Controllable multiple-step configuration transformations in a thermal/photoinduced reaction, Nat. Commun. 13 (2022) 2847.

[16] Q.-Y. Li, Y.-H. Deng, C. Cao, Y.-X. Hong, X.-R. Xue, M.-J. Zhang, Y. Ge, B. F. Abrahams, J.-P. Lang, Visible light and microwave-mediated rapid trapping and release of singlet oxygen using a coordination polymer, Angew. Chem. Int. Ed. 62 (2023) e202306719.

[17] P. Rassu, X. Ma, B. Wang, Engineering of catalytically active sites in photoactive metal–organic frameworks, Coord. Chem. Rev. 465 (2022).

[18] H.H. Mohamed, D.W. Bahnemann, The role of electron transfer in photocatalysis: fact and fictions, Appl. Catal. B 128 (2012) 91–104.

[19] L. Zhang, H.H. Mohamed, R. Dillert, D. Bahnemann, Kinetics and mechanisms of charge transfer processes in photocatalytic systems: a review, J. Photochem. Photobiol. C: Photochem. 13 (2012) 263–276.

[20] M. Dan-Hardi, C. Serre, F. Théo, R. Laurence, G. Maurin, C. Sanchez, G. Férey, A. New, Photoactive crystalline highly porous titanium(IV) dicarboxylate, J. Am. Chem. Soc. 131 (2009) 10857–10859.

[21] T. Toyao, M. Saito, Y. Horiuchi, K. Mochizuki, M. Iwata, H. Higashimura, M. Matsuoka, Efficient hydrogen production and photocatalytic reduction of nitrobenzene over a visible-light-responsive metal–organic framework photocatalyst, Catal. Sci. Technol. 3 (2013) 2092–2097.

[22] L. Shen, M. Luo, L. Huang, P. Feng, L. Wu, A clean and general strategy to decorate a titanium metal-organic framework with noble-metal nanoparticles for versatile photocatalytic applications, Inorg. Chem. 54 (2015) 1191–1193.

[23] X. Li, Y. Pi, Q. Hou, H. Yu, Z. Li, Y. Li, J. Xiao, Amorphous TiO2@NH2-MIL-125(Ti) homologous MOF-encapsulated heterostructures with enhanced photocatalytic activity, Chem. Commun. 54 (2018) 1917–1920.

[24] D. Ao, J. Zhang, H. Liu, Visible-light-driven photocatalytic degradation of pollutants over Cu-doped NH2-MIL-125(Ti), J. Photochem. Photobiol. A 364 (2018) 524–533.

[25] R.R. Solís, A. Gómez-Avilés, C. Belver, J.J. Rodriguez, J. Bedia, Microwave-assisted synthesis of NH2-MIL-125(Ti) for the solar photocatalytic degradation of aqueous emerging pollutants in batch and continuous tests, J. Environ. Chem. Eng. 9 (2021).

[26] J. Wang, A.S. Cherevan, C. Hannecart, S. Naghdi, S.P. Nandan, T. Gupta, D. Eder, Ti-based MOFs: New insights on the impact of ligand composition and hole scavengers on stability, charge separation and photocatalytic hydrogen evolution, Appl. Catal. B (283) (2021).

[27] N.S. Abdul Mubarak, K.Y. Foo, R. Schneider, R.M. Abdelhameed, S. Sabar, The chemistry of MIL-125 based materials: Structure, synthesis, modification strategies and photocatalytic applications, J. Environ. Chem. Eng. 10 (2022) 106883.

[28] Y. Wen, A. Renteria-Gomez, G.S. Day, M.F. Smith, T.H. Yan, R.O.K. Ozdemir, O. Gutierrez, V.K. Sharma, X. Ma, H.C. Zhou, Integrated photocatalytic reduction and oxidation of perfluorooctanoic acid by metal-organic frameworks: key insights into the degradation mechanisms, J. Am. Chem. Soc. 144 (2022) 11840–11850.

[29] S. Naghdi, A. Cherevan, A. Giesriegl, R. Guillet-Nicolas, S. Biswas, T. Gupta, J. Wang, T. Haunold, B.C. Bayer, G. Rupprechter, M.C. Toroker, F. Kleitz, D. Eder, Selective ligand removal to improve accessibility of active sites in hierarchical MOFs for heterogeneous photocatalysis, Nat. Commun. 13 (2022) 282.

[30] X.-M. Cheng, Y. Gu, X.-Y. Zhang, X.-Y. Dao, S.-Q. Wang, J. Ma, J. Zhao, W.-Y. Sun, Crystallographic facet heterojunction of MIL-125-NH2(Ti) for carbon dioxide photoreduction, Appl. Catal. B 298 (2021).

[31] A. Walsh, C.R.A. Catlow, Photostimulated reduction processes in a titania hybrid metal-organic framework, ChemPhysChem 11 (2010) 2341–2344.

[32] C.H. Hendon, D. Tiana, M. Fontecave, C. Sanchez, L. D'Arras, C. Sassoye, L. Rozes, C. Mellot-Draznieks, A. Walsh, Engineering the optical response of the titanium-MIL-125 metal-organic framework through ligand functionalization, J. Am. Chem. Soc. 135 (2013) 10942–10945.

[33] M.B. Chambers, X. Wang, L. Ellezam, O. Ersen, M. Fontecave, C. Sanchez, L. Rozes, C. Mellot-Draznieks, Maximizing the photocatalytic activity of metal-organic frameworks with aminated-functionalized linkers: substoichiometric effects in MIL-125-NH2, J. Am. Chem. Soc. 139 (2017) 8222–8228.

[34] M.A. Syzgantseva, N.F. Stepanov, O.A. Syzgantseva, Effect of ligand functionalization on the rate of charge carrier recombination in metal-organic frameworks: a case study of MIL-125, J. Phys. Chem. Lett. 12 (2021) 829–834.

[35] Y. Pan, J. Wang, S. Chen, W. Yang, C. Ding, A. Waseem, H.-L. Jiang, Linker engineering in metal–organic frameworks for dark photocatalysis, Chem. Sci. 13 (2022) 6696.

[36] Y.-Y. Wu, X.-W. Lu, M. Qi, H.-C. Su, X.-W. Zhao, Q.-Y. Zhu, J. Dai, Titanium–oxo cluster with 9-anthracenecarboxylate antennae: a fluorescent and photocurrent transfer material, Inorg. Chem. 53 (2014) 7233–7240.

[37] C.F.A. Negre, K.J. Young, M.B. Oviedo, L.J. Allen, C.G. Sánchez, K.N. Jarzembska, J.B. Benedict, R.H. Crabtree, P. Coppens, G.W. Brudvig, V.S. Batista, Photoelectrochemical hole injection revealed in polyoxotitanate nanocrystals functionalized with organic adsorbates, J. Am. Chem. Soc. 136 (2014) 16420–16429.

[38] T. Kramer, F. Tuna, S.D. Pike, Photo-redox reactivity of titanium-oxo clusters: mechanistic insight into a two-electron intramolecular process, and structural characterisation of mixed-valent Ti(iii)/Ti(iv) products, Chem. Sci. 10 (2019) 6886–6898.

[39] G. Capano, F. Ambrosio, S. Kampouri, K.C. Stylianou, A. Pasquarello, B. Smit, On the electronic and optical properties of metal–organic frameworks: case study of MIL-125 and MIL-125-NH2, J. Phys. Chem. C. 124 (2020) 4065–4072.

[40] K. Weissermel, H.-J. Arpe, Alcohols, in: Industrial Organic Chemistry, Wiley-VCH (Ed, 1997, pp. 191–213.

[41] T. Mallat, A. Baiker, Oxidation of alcohols with molecular oxygen on solid catalysts, Chem. Rev. 104 (2004) 3037–3058.

[42] Z. Shen, Y. Hu, B. Li, Y. Zou, S. Li, G. Wilma Busser, X. Wang, G. Zhao, M. Muhler, State-of-the-art progress in the selective photo-oxidation of alcohols, J. Energy Chem. 62 (2021) 338–350.

[43] B. Bueken, F. Vermoortele, D.E. Vanpoucke, H. Reinsch, C.C. Tsou, P. Valvekens, T. De Baerdemaeker, R. Ameloot, C.E. Kirschhock, V. Van Speybroeck, J.M. Mayer, D. De Vos, A flexible photoactive titanium metal-organic framework based on a [Ti(IV)3(mu3-O)(O)2(COO)6] cluster, Angew. Chem. Int. Ed. 54 (2015) 13912–13917.

[44] S. Smolders, T. Willhammar, A. Krajnc, K. Sentosun, M.T. Wharmby, K. A. Lomachenko, S. Bals, G. Mali, M.B.J. Roeffaers, D.E. De Vos, B. Bueken, A titanium(IV)-based metal-organic framework featuring defect-rich Ti-O sheets as an oxidative desulfurization catalyst, Angew. Chem.. Int. Ed. 58 (2019) 9160–9165.

[45] J. Castells-Gil, M.P. N, N. Almora-Barrios, I. da Silva, D. Mateo, J. Albero, H. Garcia, C. Marti-Gastaldo, De novo synthesis of mesoporous photoactive titanium (iv)-organic frameworks with MIL-100 topology, Chem. Sci., 10 (2019) 4313–4321.

[46] M.R. Hoffmann, S.T. Martin, W. Choi, D.W. Bahnemann, Environmental applications of semiconductor photocatalysis, Chem. Rev. 95 (1995) 69–96.

[47] S. Dong, J. Feng, M. Fan, Y. Pi, L. Hu, X. Han, M. Liu, J. Sun, J. Sun, Recent developments in heterogeneous photocatalytic water treatment using visible light-responsive photocatalysts: a review, RSC Adv. 5 (2015) 14610–14630.

[48] B.M. Hunter, H.B. Gray, A.M. Müller, Earth-abundant heterogeneous water oxidation catalysts, Chem. Rev. 116 (2016) 14120–14136.

[49] D. Wang, T. Sheng, J. Chen, H.-F. Wang, P. Hu, Identifying the key obstacle in photocatalytic oxygen evolution on rutile TiO2, Nat. Catal. 1 (2018) 291–299.

[50] S. Wan, J. Xu, S. Cao, J. Yu, Promoting intramolecular charge transfer of graphitic carbon nitride by donor–acceptor modulation for visible-light photocatalytic H2 evolution, Interdiscip. Mater. 1 (2022) 294–308.

[51] S.-T. Xiao, S.-M. Wu, L. Wu, Y. Dong, J.-W. Liu, L.-Y. Wang, X.-Y. Chen, Y.-T. Wang, G. Tian, G.-G. Chang, M. Shalom, P. Fornasiero, X.-Y. Yang, Confined heterojunction in hollow-structured TiO2 and its directed effect in photodriven seawater splitting, ACS Nano 17 (2023) 18217–18226.
[52] M.A. Nasalevich, C.H. Hendon, J.G. Santaclara, K. Svane, B. van der Linden, S. L. Veber, M.V. Fedin, A.J. Houtepen, M.A. van der Veen, F. Kapteijn, A. Walsh, J. Gascon, Electronic origins of photocatalytic activity in d0 metal organic frameworks, Sci. Rep. 6 (2016) 23676.
[53] J.G. Santaclara, M.A. Nasalevich, S. Castellanos, W.H. Evers, F.C. Spoor, K. Rock, L. D. Siebbeles, F. Kapteijn, F. Grozema, A. Houtepen, J. Gascon, J. Hunger, M.A. van der Veen, Organic linker defines the excited-state decay of photocatalytic MIL-125 (Ti)-type materials, ChemSusChem 9 (2016) 388–395.
[54] J.L. Mancuso, K. Fabrizio, C.K. Brozek, C.H. Hendon, On the limit of proton-coupled electronic doping in a Ti(iv)-containing MOF, Chem. Sci. 12 (2021) 11779–11785.
[55] R.W. Matthews, The radiation chemistry of the terephthalate dosimeter, Radiat. Res. 83 (1980) 27–41.
[56] J.C. Barreto, G.S. Smith, N.H.P. Strobel, P.A. McQuillin, T.A. Miller, Terephthalic acid: a dosimeter for the detection of hydroxyl radicals in vitro, Life Sci. 56 (1994) PL89–PL96.
[57] X. Qu, L.J. Kirschenbaum, E.T. Borish, Hydroxyterephthalate as a fluorescent probe for hydroxyl radicals: application to hair melanin, Photochem. Photobiol. (71 () (2000).
[58] Y. Nosaka, A.Y. Nosaka, Generation and detection of reactive oxygen species in photocatalysis, Chem. Rev. 117 (2017) 11302–11336.
[59] A. Safrany, R. Gao, J. Rabani, Optical properties and reactions of radiation induced TiO2 electrons in aqueous colloid solutions, J. Phys. Chem. B 104 (2000) 5848–5853.
[60] O. Kameneva, A.I. Kuznestov, L.A. Smirnova, L. Rozes, C. Sanchez, A. Alexandrov, N. Bityurin, K. Chhor, A. Kanaev, New photoactive hybrid organic–inorganic materials based on titanium-oxo-PHEMA nanocomposites exhibiting mixed valence properties, J. Mater. Chem. 15 (2005).
[61] A.I. Kuznetsov, O. Kameneva, A. Alexandrov, N. Bityurin, P. Marteau, K. Chhor, C. Sanchez, A. Kanaev, Light-induced charge separation and storage in titanium oxide gels, Phys. Rev. E 71 (2005) 021403.
[62] A.I. Kuznetsov, O. Kameneva, L. Rozes, C. Sanchez, N. Bityurin, A. Kanaev, Extinction of photo-induced Ti3+ centres in titanium oxide gels and gel-based oxo-PHEMA hybrids, Chem. Phys. Lett. 429 (2006) 523–527.
[63] A.I. Kuznetsov, O. Kameneva, N. Bityurin, L. Rozes, C. Sanchez, A. Kanaev, Laser-induced photopatterning of organic-inorganic TiO2-based hybrid materials with tunable interfacial electron transfer, Phys. Chem. Chem. Phys. 11 (2009) 1248–1257.
[64] H.H. Mohamed, C.B. Mendive, R. Dillert, D.W. Bahnemann, Kinetic and mechanistic investigations of multielectron transfer reactions induced by stored electrons in TiO2 nanoparticles: a stopped flow study, J. Phys. Chem. A 115 (2011) 2139–2147.
[65] J.N.H. Schrauben, Rebecca Valdez, Carolyun N., M. Braten, L. Friedley, J.M. Mayer, Titanium and Zinc Oxide Nanoparticles Are Proton-Coupled Electron Transfer Agents, Science, 336 (2012) 1298–1301.
[66] C.T. Saouma, S. Richard, S. Smolders, M.F. Delley, R. Ameloot, F. Vermoortele, D. E. De Vos, J.M. Mayer, Bulk-to-surface proton-coupled electron transfer reactivity of the metal-organic framework MIL-125, J. Am. Chem. Soc. 140 (2018) 16184–16189.
[67] M.D. Allendorf, C.A. Bauer, R.K. Bhakta, R.J.T. Houk, Luminescent metal–organic frameworks, Chem. Soc. Rev. 38 (2009).
[68] H. Guo, D. Guo, Z. Zheng, W. Weng, J. Chen, Visible-light photocatalytic activity of Ag@MIL-125(Ti) microspheres, Appl. Organo Chem. 29 (2015) 618–623.
[69] T. Devic, C. Serre, High valence 3p and transition metal based MOFs, Chem. Soc. Rev. 43 (2014) 6097–6115.
[70] A.J. Howarth, Y. Liu, P. Li, Z. Li, T.C. Wang, J.T. Hupp, O.K. Farha, Chemical, thermal and mechanical stabilities of metal–organic frameworks, Nat. Rev. Mater. 1 (2016).
[71] T.W.G. Solomons, C.B. Fryhle, S.A. Snyder. Organic Chemistry, 11th ed..,, John Wiley & Sons, Inc,, 2014.
[72] A. Shafaei, M. Nikazar, M. Arami, Photocatalytic degradation of terephthalic acid using titania and zinc oxide photocatalysts: comparative study, Desalination 252 (2010) 8–16.
[73] X.H. Lin, S.N. Lee, W. Zhang, S.F.Y. Li, Photocatalytic degradation of terephthalic acid on sulfated titania particles and identification of fluorescent intermediates, J. Hazard. Mater. 303 (2016) 64–75.
[74] V. Vaiano, G. Sarno, O. Sacco, D. Sannino, Degradation of terephthalic acid in a photocatalytic system able to work also at high pressure, Chem. Eng. J. 312 (2017) 10–19.
[75] V.C. Ferreira, A.J. Goddard, O.C. Monteiro, In situ synthesis and modification of cotton fibers with bismuthoxychloride and titanium dioxide nanoparticles for photocatalytic applications, J. Photochem. Photobiol. A 357 (2018) 201–212.
[76] D. Mateo, A. Santiago-Portillo, J. Albero, S. Navalon, M. Alvaro, H. Garcia, Long-term photostability in terephthalate metal-organic frameworks, Angew. Chem. Int. Ed. 58 (2019) 17843–17848.
[77] X. Gong, Y. Shu, Z. Jiang, L. Lu, X. Xu, C. Wang, H. Deng, Metal-organic frameworks for the exploitation of distance between active sites in efficient photocatalysis, Angew. Chem. Int. Ed. 59 (2020) 5326–5331.
[78] M. Cai, Q. Loague, A.J. Morris, Design rules for efficient charge transfer in metal–organic framework films: the pore size effect, J. Phys. Chem. Lett. 11 (2020) 702–709.
[79] P. Salvador, C. Gutierrez, The nature of surface states involved in the photo- and electroluminescence spectra of n-titanium dioxide electrodes, J. Phys. Chem. 88 (1984) 3696–3698.
[80] Y. Kakuma, A.Y. Nosaka, Y. Nosaka, Difference in TiO2 photocatalytic mechanism between rutile and anatase studied by the detection of active oxygen and surface species in water, Phys. Chem. Chem. Phys. 17 (2015) 18691–18698.
[81] R. Li, Y. Weng, X. Zhou, X. Wang, Y. Mi, R. Chong, H. Han, C. Li, Achieving overall water splitting using titanium dioxide-based photocatalysts of different phases, Energy Environ. Sci. 8 (2015) 2377–2382.
[82] Y. Nakabayashi, M. Nishikawa, N. Saito, C. Terashima, A. Fujishima, Significance of hydroxyl radical in photoinduced oxygen evolution in water on monoclinic bismuth vanadate, J. Phys. Chem. C 121 (2017) 25624–25631.
[83] Q. Huang, Y. Hu, Y. Pei, J. Zhang, M. Fu, In situ synthesis of TiO2@NH2-MIL-125 composites for use in combined adsorption and photocatalytic degradation of formaldehyde, Appl. Catal. B 259 (2019) 118106.
[84] J. Zhang, T. Bai, H. Huang, M.-H. Yu, X. Fan, Z. Chang, X.-H. Bu, Metal–organic-framework-based photocatalysts optimized by spatially separated cocatalysts for overall water splitting, Adv. Mater. 32 (2020) 2004747.
[85] R. Das, K.R. Rohit, G. Anilkumar, Recent trends in non-noble metal-catalyzed hydroxylation reactions, J. Organomet. Chem. 977 (2022) 122456.
[86] J. Hoigné, H. Bader, The role of hydroxyl radical reactions in ozonation processes in aqueous solutions, Water Res. 10 (1976) 377–386.
[87] S. Goldstein, G. Czapski, J. Rabani, Oxidation of phenol by radiolytically generated.bul.OH and chemically generated SO4.bul.-. a distinction between.bul. OH transfer and hole oxidation in the photolysis of TiO2 colloid solution, J. Phys. Chem. 98 (1994), 6586-6591.
[88] P. Salvador, On the nature of photogenerated radical species active in the oxidative degradation of dissolved pollutants with TiO2 aqueous suspensions: a revision in the light of the electronic structure of adsorbed water, J. Phys. Chem. C 111 (2007) 17038–17043.
[89] S. Gligorovski, R. Strekowski, S. Barbati, D. Vione, Environmental implications of hydroxyl radicals (•OH), Chem. Rev. 115 (2015) 13051–13092.
[90] G. Odling, N. Robertson, Why is anatase a better photocatalyst than rutile? The importance of free hydroxyl radicals, ChemSusChem 8 (2015) 1838–1840.
[91] Y. Liu, Y. Zhao, J. Wang, Fenton/Fenton-like processes with in-situ production of hydrogen peroxide/hydroxyl radical for degradation of emerging contaminants: advances and prospects, J. Hazard. Mater. 404 (2021) 124191.
[92] Z. Ye, Z. Guo, J. Wang, L. Zhang, Y. Guo, C. Yoshimura, J. Niu, Photodegradation of acebutolol in natural waters: Important roles of carbonate radical and hydroxyl radical, Chemosphere 287 (2022) 132318.
[93] S. Lee, H.-S. Bae, W. Choi, Selective control and characteristics of water oxidation and dioxygen reduction in environmental photo(electro)catalytic Systems, Acc. Chem. Res. 56 (2023) 867–877.
[94] J. Aguilera-Sigalat, A. Fox-Charles, D. Bradshaw, Direct photo-hydroxylation of the Zr-based framework UiO-66, Chem. Commun. 50 (2014) 15453–15456.
[95] H. Huang, X.-S. Wang, D. Philo, F. Ichihara, H. Song, Y. Li, D. Li, T. Qiu, S. Wang, J. Ye, Toward visible-light-assisted photocatalytic nitrogen fixation: a titanium metal organic framework with functionalized ligands, Appl. Catal. B 267 (2020).
[96] J. He, F. Xu, Y. Tian, C. Li, X. Hou, Atmospheric low-temperature plasma for direct post-synthetic modification of UiO-66, Chem. Commun. 56 (2020) 5803–5806.